

Internal dynamics and elasticity of confined entropic gels

E. K. Hobbie and A. D. Stewart*

National Institute of Standards and Technology, Gaithersburg, Maryland 20899

(Received 5 November 1999; revised manuscript received 19 January 2000)

The internal dynamics and elasticity of colloidal gels formed via depletion in confined nearly hard-sphere mixtures are studied via particle-tracking measurements of the self part of the van Hove correlation function, which is found to decay exponentially in space and exhibit a scaling in terms of its first moment. The second moment, or mean-square particle displacement, exhibits a stretched-exponential decay to a plateau and provides a measure of the weak elastic modulus of the gel. A Fourier analysis of the real-space probability distribution yields the intermediate scattering function, which at fixed wave vector exhibits a stretched exponential decay to a nonzero plateau, reminiscent of dynamic behavior observed in a broad class of disordered systems.

PACS number(s): 82.70.Dd, 63.50.+x, 82.70.Gg

I. INTRODUCTION

Particle motion in disordered systems is a theme connecting a broad range of topics in condensed matter physics. Phenomena as diverse as the conformational motion of proteins [1], the transport of charge in amorphous semiconductors [2], and the kinetics of glass forming liquids [3], as well as structural relaxation in gels [4,5], confined liquid crystals [6], and defective crystalline solids [7], can exhibit similar dynamic behavior, such as temporal decays that are stretched-exponential rather than exponential, that can often be linked to disorder in the form of a broad distribution of length, time, or energy scales. In the case of gels, the particles form remarkably fragile networks of amorphous clusters that can often be described as fractal over a significant window of size, and recent dynamic light scattering measurements performed on fractal colloidal gels have been used to extract information about the weak network elasticity from a simple model of segmental motion within the gel [4]. Such *equilibrium* methods of probing the elasticity of random networks are well suited for measuring the properties of extremely fragile systems, for which conventional rheological techniques prove quite difficult.

Here, video microscopy is used to study the internal dynamics and elasticity of gels formed via depletion in confined nearly-hard-sphere binary mixtures. Because the depletion bond that forms between sedimented colloidal particles immersed in a solution of much smaller colloidal particles is relatively weak (typically on the order of $5 k_B T$), the quasi-two-dimensional gels that form in these mixtures are remarkably fragile. From the space-time trajectories of the larger particles that comprise the confined gel, we compute dynamic density-density correlation functions in both real and reciprocal space. The self part of the van Hove function, which is found to decay exponentially in space and exhibit a scaling in terms of the mean particle displacement, is used to extract a measure of the weak elasticity of the gel based on an extension of the model proposed in Ref. [4]. The interme-

mediate scattering function, which is obtained from a Fourier analysis of the real-space data, exhibits a stretched-exponential decay to a nonzero plateau, reminiscent of behavior observed in a variety of disordered systems [3–6], which can be viewed as a direct consequence of the space-time evolution of the real-space van Hove function. The results may offer new insight into the general topic of strongly caged motion in complex and disordered systems.

II. EXPERIMENTAL BACKGROUND

Binary suspensions of polystyrene spheres with diameters $a_L = 2.9 \mu\text{m}$ and $a_S = 213 \text{ nm}$ were prepared at fixed large-sphere volume fraction $\phi_L \approx 0.025$ for small-sphere volume fractions $\phi_S \approx 0.20, 0.25,$ and 0.30 [8]. The particles are stabilized with a charged polymer surfactant, and enough salt is added to the aqueous solution (0.01 M) to screen the bare pair potential to short-range repulsive. The large spheres aggregate in the presence of the much more numerous small spheres via a *depletion* mechanism. Because the latter are excluded from a shell of volume (width $a_S/2$) surrounding each large sphere, the effective small-sphere volume fraction, and hence the entropic free energy of the nearly hard-sphere host fluid, decreases when two or more large spheres come into contact, driving a thermodynamic phase separation into coexisting large-sphere rich and large-sphere poor phases [9]. The effective potential between neighboring large spheres has been measured [10], making these mixtures model systems for fundamental studies of segregation and crystallization.

The sample cell is an epoxy-sealed microscope slide and cover slip with $25\text{-}\mu\text{m}$ wire spacers. The large spheres are gravitationally confined to the surface of the glass slide, leading to trajectories that are approximately two dimensional [11], and one hour after mixing they form an amorphous network (Fig. 1). For isolated clusters formed under moderate quenches ($\phi_S < 0.30$), previous work suggests that this amorphous phase is metastable with respect to a close-packed crystal [11]. For the connected clusters of interest here, the $\phi_S \approx 0.20$ samples eventually condense into aggregates of randomly oriented crystallites, while the $\phi_S \approx 0.25$ and 0.30 samples remain amorphous at late times, suggesting

*Present address: Department of Physics, Southern University, Baton Rouge, LA 70813.

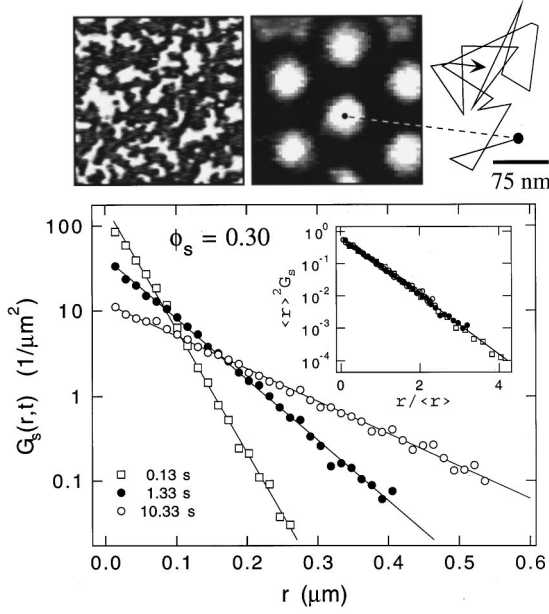


FIG. 1. One hour after mixing (upper panel), the large spheres form a network of connected clusters (upper left, width = 140 μm , $\phi_S \approx 0.30$) with a close-packed amorphous structure (upper middle, width = 8 μm). Each large sphere vibrates in a cage formed by its nearest neighbors (upper right, time interval for each step = 0.27 s). Log-linear plot of $G_S(r,t)$ vs r at different correlation times, where the fits are as described in the text. The inset shows the scaling of $G_S(r,t)$ with its first moment, $\langle r \rangle$.

that an increase in the local density of large spheres at the bottom surface of the sample cell, relative to that used in a previous study [11], might lead to a suppression of crystallization in these mixtures.

Due to thermal fluctuations, large spheres in the gel undergo small-amplitude Brownian-like motion (Fig. 1). To study these structural vibrations, video sequences (100 \times objective, 2 \times CCD camera) were recorded at different regions of the sample to obtain ensembles of several thousand large-sphere trajectories, $\mathbf{r}_i(t)$. Measurements were taken 1 and 20 h after mixing at each ϕ_S , and each video frame contains on the order of 400 large-sphere centers, with an accuracy of around 20 nm [12]. The particles are tracked for an interval of roughly 10 s (on the order of 200 small-sphere diffusion times), which corresponds to several cycles of the fast motion of interest. Free large spheres and small, isolated clusters were analyzed separately. In all cases, large-sphere structures that form over the course of time, crystalline or amorphous, are easily sheared apart by gently compressing the cover slip of the sample cell, which essentially ‘‘melts’’ the large spheres back to a metastable fluid state.

III. ANALYSIS

A quantity of fundamental interest that is directly tabulated from the particle trajectories is the self part of the van Hove correlation function, $G_S(r,t)$, which is the propagator or Green function for self-diffusion in the gel. The quantity $P(r) = 2\pi r G_S(r,t) \Delta r$ is the probability that a large sphere has moved a distance r in a time interval t , with the normalization $\sum_r P(r) = 1$ and the bin size $\Delta r = 15 \text{ nm}$. Moments of this distribution give the mean particle displacements as a

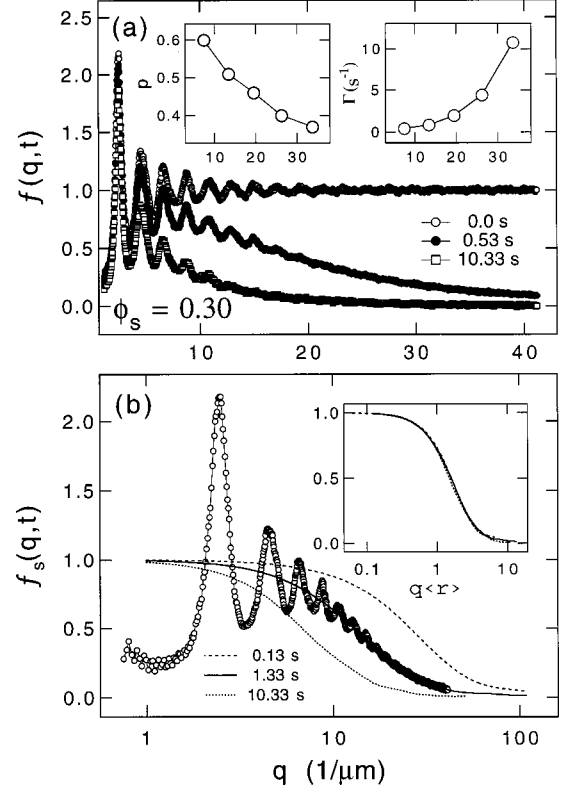


FIG. 2. (a) $f(q,t)$ vs q for the data shown in Fig. 1, where the signal at fixed q decays in time via Eq. (2) with $p(q)$ and $\Gamma(q)$ as shown in the insets. (b) Linear-log plot of $f_S(q,t)$ vs q , where $f(q,t)$ (markers) is shown for reference at $t = 1.33 \text{ s}$. The inset shows the scaling of $f_S(q,t)$ with $\langle r \rangle$.

function of time. Figure 1 shows $G_S(r,t)$ vs r as a function of time for $\phi_S \approx 0.30$ in the early stages of phase separation (1 h after mixing), and suggests that $G_S(r,t)$ can be well approximated by an exponential decay in r (solid lines, Fig. 2) over the length scales probed in this study. This striking behavior is in contrast to that exhibited by a single Brownian particle, either freely diffusing or trapped in a harmonic potential, for which $G_S(r,t)$ is a Gaussian in r [13].

An interesting feature of the data is an apparent scaling of $G_S(r,t)$ in terms of its first moment, $\langle r(t) \rangle$, the mean particle displacement. As shown in the inset to Fig. 1, the data follow the scaling relation

$$G_S(r,t) \sim \langle r \rangle^{-2} \exp(-cr/\langle r \rangle), \quad (1)$$

where $c \approx 2$ for all of the quench depths (ϕ_S) and annealing times considered [normalization then gives the dimensionless prefactor in Eq. (1) to be $c^2/2\pi \approx 0.65$]. The importance of the first moment is somewhat reminiscent of the scaling behavior observed in simulations of fractal-time random walks, a model originally used to study transport in amorphous semiconductors [14].

Figure 2(a) shows the intermediate scattering function,

$$f(q,t) = N^{-1} \langle \sum_{jk} \exp\{-i\mathbf{q} \cdot [\mathbf{r}_j(t) - \mathbf{r}_k(0)]\} \rangle$$

for $\phi_S \approx 0.30$ in the early stages of phase separation (1 h after mixing), where the indices j and k run over the large-sphere coordinates of a single frame, and the brackets denote an

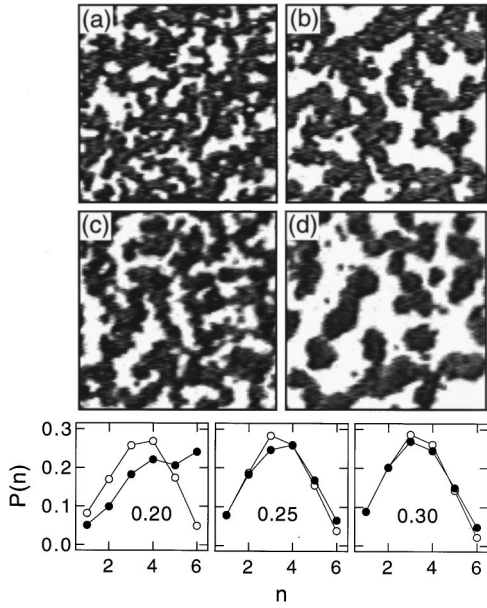


FIG. 3. Normalized bond-number distribution for different quench depths in the early (1 h after mixing, open markers) and late (20 h after mixing, closed markers) phases. Error bars are the size of the data markers. The micrographs show the coarse-grained morphology (width=140 μm) for $\phi_S \approx 0.30$ (a) 1 and (b) 20 h after mixing, and for $\phi_S \approx 0.20$ (c) 1 and (d) 20 h after mixing.

ensemble average over many frames. The data are plotted as a function of the wave vector (q) with each curve representing a different correlation time (t). A common feature revealed by dynamic light scattering from gels is a stretched-exponential temporal decay of $f(q, t)$ to a nonzero plateau reflecting the nonergodic, strongly-caged motion of each segment within the gel [4,5]. The data in Fig. 1(a) are well described by

$$f(q, t) = f_\infty(q) + \{S(q) - f_\infty(q)\} \exp[-(\Gamma t)^p], \quad (2)$$

with fitting parameters $f_\infty(q)$, $\Gamma(q)$ [right inset, Fig. 2(a)], and $p(q)$ [left inset, Fig. 2(a)]. For $q > 10 \mu\text{m}^{-1}$, the decay rate $\Gamma(q)$ scales as $q^{2.8}$, which bears a striking resemblance to behavior observed in dilute polymer solutions [15]. As shown in Fig. 2(b), the signal is also dominated by the self term,

$$f_S(q, t) = N^{-1} \langle \sum_k \exp[-i\mathbf{q} \cdot (\mathbf{r}_k(t) - \mathbf{r}_k(0))] \rangle$$

somewhat reminiscent of behavior observed in concentrated colloidal suspensions [16].

The above two observations might simply reflect the fact that motion in these gels is strongly ‘‘caged,’’ occurring over length scales smaller than a large-sphere diameter, which might explain the dominance of the self term, and much smaller than the size of a typical cluster, which might explain the q dependence of the decay rate at short wavelengths. The potential relevance of the latter observation might be inferred from an argument related to the dynamic structure factor of dilute polymer solutions, which suggests that if the long-wavelength (low- q) decay rate is (Stokes-Einstein) diffusive, the high- q decay rate, which must be independent of molecular weight (or in our case cluster size), must scale as q^3 [15].

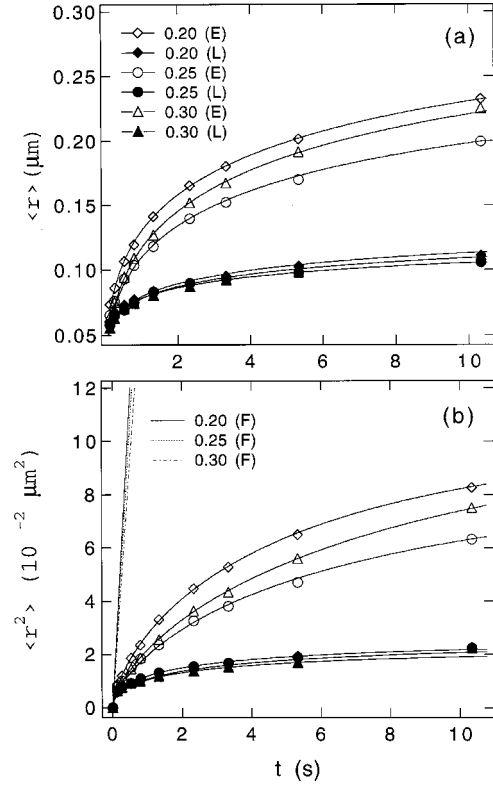


FIG. 4. (a) Mean displacement vs time for different quench depths in the early (E) and late (L) phases, and (b) mean-square displacement vs time for different quench depths in the early and late phases, where the fits are as described in the text. In (b), the steep lines on the left are diffusion curves for free (F) large spheres at each ϕ_S .

We also note that the behavior represented by Eq. (2) might simply be viewed as a direct consequence of the specific space-time evolution of the self part of the real-space van Hove function (and its moments, which we focus on below).

IV. MOMENTS OF THE DISTRIBUTION

Changes in the local dynamics with quench depth (ϕ_S) and annealing time are contained in the moments of $G_S(r, t)$. The gels coarsen over the course of 20 h (micrographs, Fig. 3), which is evident in $P(n)$, the probability of finding a large sphere in the gel with n nearest neighbors (lower panel, Fig. 3). For $\phi_S \approx 0.20$, crystallization is evident as a shift in the most probable value of n from around 3 or 4 (early phase) to around 6 (late phase). For $\phi_S \approx 0.25$ and 0.30, there is a *subtle* shift toward higher n that reflects the coarsening of the domains, but the distribution remains peaked around $n = 3$ or 4. These shifts are evident in the mean bond number

$$\langle n \rangle = \sum_{n=1}^6 nP(n), \quad (3)$$

which evolves from the early to late phases as; $\langle n \rangle = 3.43$ (early) to 4.15 (late) for $\phi_S = 0.20$, $\langle n \rangle = 3.34$ (early) to 3.44 (late) for $\phi_S = 0.25$, and $\langle n \rangle = 3.23$ (early) to 3.31 (late) for $\phi_S = 0.30$. The time dependence of $\langle r \rangle$ varies among the different morphologies [Fig. 4(a)] and is well described by a stretched-exponential decay to a plateau [solid curves, Fig.

4(a)], however there is considerable variation in the stretching exponent as a function of quench depth and annealing time. Information about the gel elasticity is contained in the second moment, or the mean-square displacement, which we discuss in detail below. We also note that the time dependencies of the mean particle displacement and the root-mean-square displacement are virtually identical.

In the model of Krall and Weitz [4], thermal fluctuations in a gel span a wide range of length scales, and the motion of a particle often arises from the collective motion of the cluster to which it is attached. A localized mode of diameter s is modeled as a Brownian particle in a harmonic potential [13] with a spring constant $\kappa(s) = \kappa_0(a_L/s)^\beta$ and a relaxation time $\tau(s) = k_B T(s/a_L)/D\kappa(s)$, where D is the diffusion coefficient of a free large sphere [4]. The mean-square displacement is obtained by summing the contributions from all modes s , which can be evaluated numerically and is well represented by the expression [4]

$$\langle r^2(t) \rangle \approx \delta^2 \{1 - e^{-(t/\tau_0)^p}\}, \quad (4)$$

with $p = \beta/(\beta + 1)$, $\tau_0 \sim \tau(R)$, where R is the characteristic length scale of the gel or the mean cluster dimension, and $\delta^2 \approx 2d_f k_B T(R/a_L)^\beta / \beta \kappa_0$, where d_f is the fractal dimension of the gel [17]. The elastic modulus is given approximately by [4] $E \approx 2d_f k_B T / \beta R \delta^2$. The physical motivation for the model is that the gel appears the most rigid at the shortest length scales, with $\kappa(a_L) = \kappa_0$, and the decrease in rigidity with increasing length scale is modeled as a power-law decay with an exponent β . The trajectories encountered here are essentially two dimensional, which makes our system significantly different from that originally modeled in Ref. [4]. We note, however, that for a Brownian harmonic oscillator, the quantity that varies with spatial dimension is the propagator; the mean-square displacement has the same time dependence [13]. The exponent β , which in principle might be sensitive to confinement and thus the effective dimensionality, is determined from a fit of the data to Eq. (4), and the fractal dimension is determined independently [17].

Figure 4(b) shows $\langle r^2 \rangle$ vs t , where the curves are fits of the data to Eq. (4). Also shown are the diffusion curves (straight lines) obtained from ensembles of free large spheres at each ϕ_S . For the early phase data, $p = 0.70$ (implying $\beta = 2.33$) and $\tau_0 \sim 5 - 10$ s with $E \approx 0.015, 0.019, \text{ and } 0.016$ dyn/cm² for $\phi_S \approx 0.20, 0.25, \text{ and } 0.30$, respectively. Interestingly, the value of the exponent p is in reasonable agreement with the value reported elsewhere [4]. Using the order-of-magnitude estimate $E \sim \langle n \rangle \Delta / a_L^3$, we obtain an estimate of the depth of the effective potential well between adjacent large spheres; $\Delta / k_B T \sim 2.6, 3.4, 3.0$ for $\phi_S \approx 0.20, 0.25, \text{ and } 0.30$, respectively. For two large spheres in contact on a smooth surface, simple geometry shows that the depletion cavity extends down from the plane of common center a distance

$$(a_L/2) \sqrt{2a_S/a_L + (a_S/a_L)^2} \approx 0.2a_L,$$

so that the nature of the depletion attraction between adjacent confined large spheres should be comparable to that in the bulk, provided ϕ_S is homogeneous near the wall. The values we infer are smaller than those measured by Crocker *et al.*

[10]; $\Delta / k_B T \sim 4, 5.6, \text{ and } 5$ for $\phi_S \approx 0.20, 0.25, \text{ and } 0.30$, respectively, which could be explained by noting that 1 h after mixing the large-sphere structures may not have relaxed completely into their primary depletion minima.

For the late-phase data, $p = 0.50$ and $\tau_0 \sim 2 - 3$ s with $E \approx 0.12, 0.12, \text{ and } 0.17$ dyn/cm² for $\phi_S \approx 0.20, 0.25, \text{ and } 0.30$, respectively, roughly an order of magnitude larger. Note that $p = 0.5$ implies $\beta \approx 1$, which suggests that the annealed gels appear relatively stiff at large length scales. Estimates of the depth of the effective depletion well obtained from these elastic constants are $\Delta / k_B T \sim 17.3, 20.9, 30.8$ for $\phi_S \approx 0.20, 0.25, \text{ and } 0.30$, respectively, considerably larger than those cited above. This enhanced rigidity may be due to confinement effects and warrants further investigation. Regardless, these networks are among the weakest materials found in nature, with elastic moduli almost four orders of magnitude smaller than values previously reported for a colloidal gel at a comparable volume fraction [4], a simple consequence of the large size of the particles and the weak attraction between them.

V. CONCLUSION

In the above picture, a superposition of the mean-square displacements of all the localized overdamped modes of the gel, each of which relaxes exponentially to a plateau with a time constant unique to the size of that mode, is what leads to the stretched-exponential dynamics [4]. It is interesting to note that the analogous superposition of the corresponding Gaussian propagators leads to a spatial decay of $G_S(r, t)$ that appears approximately exponential at large r [18]. Given the potential relevance to the general phenomena of strongly caged motion in disordered and glassy systems, more theoretical work is needed. The complex free-energy landscapes associated with multiple metastable minima and the glassy dynamics associated with confinement may make these mixtures particularly well suited for studying the dynamics of localized fluctuations in disordered systems.

A puzzling feature the data is the apparent increase in the effective depth of the depletion-potential well between neighboring large spheres upon annealing. One possibility is that gravitational confinement of the larger structures restricts segmental motion (perhaps due to increased wall friction), suppressing the mean-square displacements, and making the gels appear artificially rigid. Another possibility is that the thermal motion within the larger, collective structures becomes reduced as the clusters settle into a depletion well that exists between large particles and the wall [19], effectively supplementing the gravitational confining force, although we did not discern any change in the mobility of isolated, free large spheres as a function of annealing time. This apparently enhanced rigidity is also consistent with the measured decrease in the exponent p upon annealing, which implies that clusters would appear more rigid at longer length scales. The fact that the modulus of the crystalline phase does not differ radically from those inferred for the two amorphous annealed phases is also puzzling, but might be explained by the fact that upon crystallization the clusters become somewhat disconnected [compare Figs. 3(c) and 3(d)], freeing degrees of freedom associated with cluster rotation, enhancing the mean-square displacement, and thus

making the solid appear artificially soft. Possible directions for future work include bulk particle-tracking measurements performed on buoyancy matched samples, both in equilibrium and in externally imposed shear fields.

ACKNOWLEDGMENT

This work was supported in part by the National Science Foundation.

-
- [1] See, for example, H. Frauenfelder, S. G. Sligar, and P. G. Wolynes, *Science* **254**, 1598 (1991), and references therein.
- [2] See, for example, H. Scher, M. F. Shlesinger, and J. T. Bendler, *Phys. Today* **44**, 26 (1991).
- [3] See, for example, M. D. Ediger, C. A. Angell, and S. R. Nagel, *J. Phys. Chem.* **100**, 13 200 (1996) and references therein.
- [4] A. H. Krall and D. A. Weitz, *Phys. Rev. Lett.* **80**, 778 (1998).
- [5] S. Z. Ren and C. M. Sorensen, *Phys. Rev. Lett.* **70**, 1727 (1993).
- [6] M. Copic and A. Mertelj, *Phys. Rev. Lett.* **80**, 1449 (1998).
- [7] E. Rabani, J. D. Gezelter, and B. J. Berne, *Phys. Rev. Lett.* **82**, 3649 (1999).
- [8] Relative small-sphere volume fractions (± 0.01) were measured by weighing samples before and after drying in a vacuum oven.
- [9] See, for example, M. Dijkstra, R. van Roij, and R. Evans, *Phys. Rev. E* **59**, 5744 (1999), and references therein.
- [10] J. C. Crocker, J. A. Mateo, A. D. Dinsmore, and A. G. Yodh, *Phys. Rev. Lett.* **82**, 4352 (1999); R. Verma, J. C. Crocker, T. C. Lubensky, and A. G. Yodh, *Phys. Rev. Lett.* **81**, 4004 (1998).
- [11] E. K. Hobbie, *Phys. Rev. Lett.* **81**, 3996 (1998); E. K. Hobbie, *Langmuir* **15**, 8807 (1999).
- [12] The spatial resolution was determined by grabbing the same frame repeatedly and tabulating the probability density $rG_S(r)$ with respect to one of the frames, and by grabbing consecutive frames (0.33 s interval) of fixed microscopic objects (dried colloids) and tabulating $rG_S(r)$ with respect to the first frame, both of which are sharply peaked around $r=15-20$ nm.
- [13] M. Doi and S. F. Edwards, *The Theory of Polymer Dynamics* (Oxford University Press, Oxford, 1986).
- [14] S. Gomi and F. Yonezawa, *Phys. Rev. Lett.* **74**, 4125 (1995); H. Scher and E. W. Montroll, *Phys. Rev. B* **12**, 245 (1975).
- [15] P. G. de Gennes, *Scaling Concepts in Polymer Physics* (Cornell University Press, Ithaca, 1979); M. Adam and M. Del-santi, *Macromolecules* **10**, 1229 (1977); C. C. Han and A. Z. Akcasu, *ibid.* **14**, 1080 (1981).
- [16] P. N. Segré and P. N. Pusey, *Phys. Rev. Lett.* **77**, 771 (1996).
- [17] We use $d_f=1.7$ for the gels described here, a value suggested by an analysis of isolated amorphous-phase clusters [11].
- [18] E. K. Hobbie (unpublished).
- [19] See, for example, D. Rudhardt, C. Bechinger, and P. Leiderer, *Phys. Rev. Lett.* **81**, 1330 (1998).